ARCHIVES OF METALLURGY AND MATERIALS
Volume 52 2007 Issue 1

C. HAMILTON*, S. DYMEK** , M. BLICHARSKI**

MECHANICAL PROPERTIES OF Al 6101-T6 WELDS BY FRICTION STIR WELDING AND METAL INERT GAS WELDING

WŁASNOŚCI MECHANICZNE SPOIN STOPU Al 6101-T6 WYKONANYCH METODĄ TRADYCYJNĄ ORAZ METODĄ TARCIOWĄ Z MIESZANIEM MATERIAŁU

Aluminum 6101-T6 extrusions are commonly used to distribute electricity in commercial structures due to their excellent conductivity and resistance to corrosion. When the building configuration demands a bend in the electrical pathway, the extrusions must be welded together at a 90° angle, forming a corner weld. The most widely used joining technique is fusion welding; however, this process typically restricts material flow in a factory due to the manual labor involved. In response, a leading manufacturer of electrical pathways, replaced their conventional Metal Inert Gas (MIG) welding with Friction Stir Welding (FSW). This investigation compared the mechanical performance of 6101-T6 corner welds produced through the FSW and MIG welding and correlated the tensile properties and fracture characteristics with the weld microstructures. FSW produced higher quality welds with superior mechanical properties that failed through typical ductile rupture. All FSW tensile specimens failed on the retreating side of the weld, and the FSW nugget revealed a consistent grain size of 10 μm to 20 μm with a non-uniform distribution of secondary phase particles creating a banded appearance.

Keywords: friction stir welding, aluminum, microstructure, mechanical properties

Stopy Al typu 6101-T6, z uwagi na ich dobre przewodnictwo i odporność korozyjną, są często używane w postaci walcowanych płyt jako przewodniki prądu elektrycznego w zastosowaniach komercyjnych, gł. w rozdzielniach prądu. Niektóre rozwiązania konstrukcyjne wymagają łączenia takich płyt pod kątem 90°. Najczęściej stosowaną techniką łączenia jest spawanie ogniowe, jednak ten proces łączenia ma liczne wady, tak w odniesieniu do samych stopów aluminium, jak i zaangażowania ludzkiej pracy. Spowodowało to zastąpienie tradycyjnego spawania przez łączenie tarciowe z mieszaniem materiału (friction stir welding – FSW). Obecne badania mają na celu wykazanie wyższości połączeń wykonanych metodą FSW nad połączeniami tradycyjnymi. W pracy dokonano porównania własności mechanicznych oraz mikrostruktury połączeń obu typów. Wykazano, że metoda tarciowego łączenia z mieszaniem materiału prowadzi do wykonania połączeń lepszej jakości pod względem własności mechanicznych. Wszystkie próbki łączone metodą FSW pękały podczas próby rozciągania po stronie spływu (retrieting side) spoiny. W mikrostrukturze spoiny występowały ziarna o wielkości ok. 10–20 μm oraz cząstki innej fazy ułożone w charakterystyczne pasma.

1. Introduction

Invented in 1991 by The Welding Institute, Friction Stir Welding (FSW) is a novel solid-state joining process that is gaining popularity in the manufacturing sector [1, 2]. FSW utilizes a rotating tool design to induce plastic flow in the base metals and to essentially "stir" them together. During the welding process, a pin, attached to the primary tool, is inserted into the joint with the shoulder of the rotating tool abutting the base metals as shown in Figure 1. As the tool traverses the joint, the rotation of the shoulder under the influence of an applied, fixed load heats the metal surrounding the joint and with the rotating action of the pin induces metal from each workpiece to flow together and form the weld. The microstructure resulting from the influence of plastic deformation and elevated temperature is generally a complex array of fine, recrystallized grains. The joint, however, is fundamentally defect-free and displays excellent mechanical performance when compared to conventional fusion welds. Over the last fifteen years, numerous investigations have sought to characterize the principles of FSW and to model the microstructural development. The majority of these investigations pertaines to heat treatable aluminum (2xxx, 6xxx and 7xxx series) [3–6] and were stimulated by the complex evolution of

* MIAMI UNIVERSITY, DEPARTMENT OF MECHANICAL AND MANUFACTURING ENGINEERING, KREGER HALL, OXFORD, OH 45056, USA
** FACULTY OF METALS ENGINEERING AND INDUSTRIAL COMPUTER SCIENCE, AGH UNIVERSITY OF SCIENCE AND TECHNOLOGY, 30-059 KRAKÓW, AL. MICKIEWICZA 30, POLAND

microstructure (and thus properties) in these alloys during the FSW process. The current status of FSW research has been well summarized by Mishra and Ma [7]. Despite these efforts, however, material behavior associated with FSW remains undefined and presents a fruitful avenue of continued research.

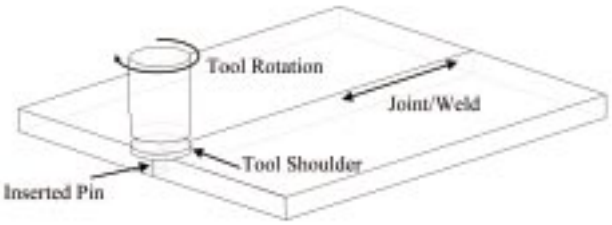

Fig. 1. Schematic representation of the friction stir welding process and tool geometry

Since no melting occurs during FSW, the process is performed at much lower temperatures than traditional welding techniques, such as Metal Inert Gas (MIG), and circumvents many of the environmental and safety issues associated with traditional welding methods. In addition, FSW has been shown to successfully weld aluminum alloys, historically considered difficult to fusion weld, with higher joint efficiencies than conventional methods [8–10]. Due to these benefits, the manufacturing sector is embracing FSW as a new technology and replacing fusion weld capabilities. Though the aerospace industry is the primary lead in adopting FSW, other industrial segments are following their example. One such company is a major manufacturer of aluminum electrical pathways, "busbars", and though much of their FSW tool design and process parameters remain proprietary, a comparison of aluminum 6101-T6 extrusions welded by FSW and MIG welding forms the basis of this research investigation.

Aluminum 6101-T6 extrusions are commonly used in the electrical busbar industry due to their excellent electrical conductivity and resistance to corrosion. The major alloying elements of aluminum 6101 are magnesium and silicon at 0.6 wt% and 0.5 wt%, respectively, with iron present as impurity up to 0.5 wt% [11]. These busbar extrusions distribute high amperage (in excess of 400 A) to various locations within buildings or similar structures; however, when the building configuration demands a bend in the electrical pathway, the busbars must be welded together at a 90° angle, forming a corner weld. This configuration is somewhat unique to FSW research as most studies have concentrated on butt welds for which welding occurs along the longitudinal direction of both workpieces (extrusion or plate) [7]. In the corner weld, however, welding occurs along the longitudinal (L) direction of one extrusion and along the long-transverse (LT) direction of the other. As shown in Figure 2, with a clockwise tool rotation FSW occurs along the L-direction of the advancing side (rotation of the tool is in the same direction as the weld direction) and along the LT-direction of the retreating side (rotation of the tool is in the opposite direction of the weld direction). The following investigation compares the mechanical performance of 6101-T6 corner welds achieved through the FSW and MIG processes and correlates the tensile properties and fracture behavior with the microstructural characteristics inherent in each welding technique.

2. Experimental procedure

To compare the metal inert gas and the friction stir welding processes, aluminum 6101-T6 extrusions produced in accordance with ASTM B 317 with a thickness of 6.35 mm and a width of 154 mm were obtained and welded in the corner configuration represented in Figure 2 [11]. All welding was performed by the aforementioned electrical busbar company following their internal, standard operating procedures. The specialists producing the MIG welded samples used "best practice" techniques and created fusion welds typical of the manufacturing process. Specific details of the FSW tool design and operating parameters remain proprietary to the busbar firm; however, the aluminum extrusions were friction stir welded with a tool rotation speed of 900 rpm, a traverse speed in the weld direction of 5 mm/s and an applied load of 2250 kN. Mishra and Ma have reviewed many of the common FSW tool designs whose characteristics are indicative of the current technique under investigation [7, 12, 13].

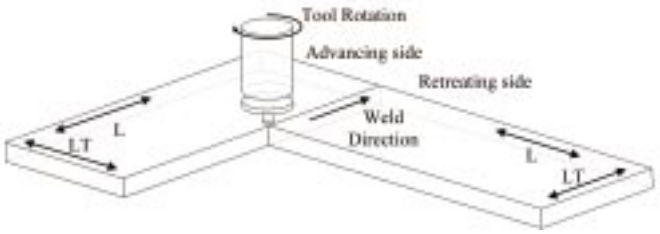

Fig. 2. Schematic of corner weld geometry and FSW orientation

Full thickness (6.35 mm) tensile samples were then excised from the MIG and FSW corner welds as shown in the plan view of Figure 3. With this specimen orientation, the weld is centered along the tensile specimen, and as such, the load is applied transverse to the weld direction and across all microstructural regions associated with the welding process, i.e. the weld nugget, the heat affected zone (HAZ) and the thermo-mechanically affected zone (TMAZ) distinctive to FSW. The geometry and dimensions of the welded tensile specimens

are shown in Figure 3 with the longitudinal direction indicated. During tensile testing, therefore, the tensile load is applied in the LT-direction along one side of the specimen (the advancing side during FSW) and in the L-direction along the other side (the retreating side during FSW). In addition to the welded tensile specimens, tensile bars of the same geometry and dimensions were also excised in the L-direction from an area well away from the weld region for baseline property comparison.

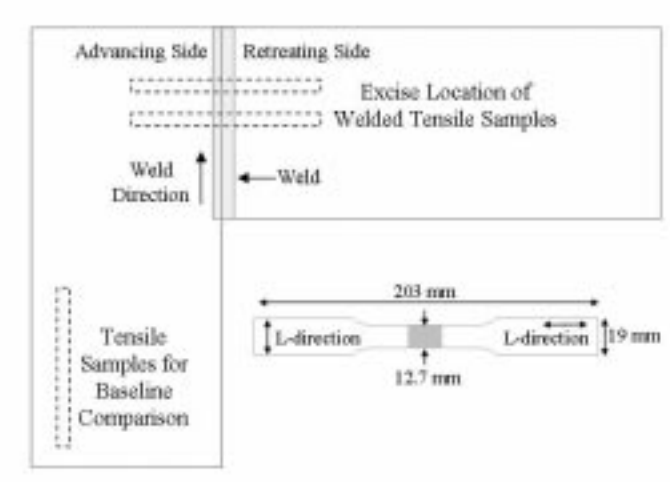

Fig. 3. Tensile specimen excise location with specimen geometry and dimensions

All tensile tests were performed in accordance with ASTM E 8 utilizing an Instron 5867 screw driven test frame with a 30 kN load cell and a 0.001–500 mm/min speed range [14]. Specimen extension, crosshead deflection and load were recorded throughout the test duration. Specimen extension was measured by means of a 25.4 mm extensometer attached to the reduced section that spanned the width of the weld when present. The extensometer remained attached to the specimen through yielding, but was removed prior to specimen failure to prevent damage to the equipment. The yield stress, σ_y, was obtained by the 0.2% offset method, and the elastic modulus, E, was determined by fitting a linear regression to the elastic region of the stress-strain curve. Elongation was determined by the extent of crosshead deflection and the initial length of the specimen between the machine grips. A minimum of four replicate tests were executed for each welding condition, and a minimum of three replicate tests were performed for the baseline material. To correlate the measured mechanical properties with the microstructural characteristics of the weld processes, welds were examined by light, and fracture surfaces by scanning electron microscopies. The grain size was evaluated from light microscope images by the mean linear intercept method.

3. Results

Table 1 summarizes the average mechanical properties for the welded tensile specimens and the baseline material. Both weld samples, MIG and FSW, show an approximate 35% decrease in the average ultimate tensile strength, σ_{UTS}, when compared to the L-direction baseline properties, but the most significant reduction in mechanical performance is recorded in the yield stress and elongation. For the MIG welded samples, the yield stress fell to an average value of 62 MPa, a 64% reduction in strength when compared to the L-direction baseline properties. The average yield stress of the FSW specimens also significantly fell from the baseline value, though not to the same extent as the MIG welded specimens. For the FSW specimens, the yield stress decreased 60% from the L-direction baseline value to 69 MPa.

TABLE 1
Average mechanical properties of each weld condition and baseline material

Material	Yield Stress σ_y (MPa)	Ten. Strength σ_{TS} (MPa)	Modulus E (GPa)	Elongation e (%)
Non-weld (L)	174	200	65	9.4
FSW	69	130	64	3.4
MIG	62	126	51	1.9

Figure 4 displays typical stress-strain curves for each test condition. Though certainly showing a decrease in the mechanical properties, the curve of the FSW specimen still reveals a distinct elastic regime that is followed by permanent deformation at approximately 0.2% strain. In contrast, the stress-strain curve for the MIG welded specimen shows very little elasticity, but gives way to plastic deformation almost immediately upon loading. This result is not necessarily surprising given the melting and resolidification that occurs during fusion welding, as well as the usual presence of contaminants and filler material in the weld. This lack of elasticity is evident in the value for the elastic modulus determined for the MIG welding process and in the small amount of elongation measured in these specimens. The average elongation of the MIG welded samples was slightly less than 2% underscoring a profound loss in ductility from the base line condition. The FSW specimens also showed a decrease in the average elongation from the baseline value, 9.4% against 3.4%, but demonstrate that a weld produced through FSW retains a higher degree of ductility than a weld manufactured through conventional fusion processes.

Examination of the MIG welded fracture surfaces through scanning electron microscopy reveals a high level of porosity in the weld and few features characteristic

of ductile rupture. Figure 5 is an SEM micrograph of a representative MIG welded fracture surface of 6101-T6 aluminum alloy. Dominating the micrograph are the numerous voids ranging in diameter from 50 μm to 200 μm. The ligaments between the porosity show features more indicative of brittle fracture than ductile rupture, an observation consistent with the reduced ductility noted during mechanical testing. Due to the high temperatures required for fusion welding and the subsequent melting and solidification that occur, voids are common defects found in fusion welds. The presence of voids in the MIG welds contributes to the reduced mechanical properties and poor elongation observed during testing.

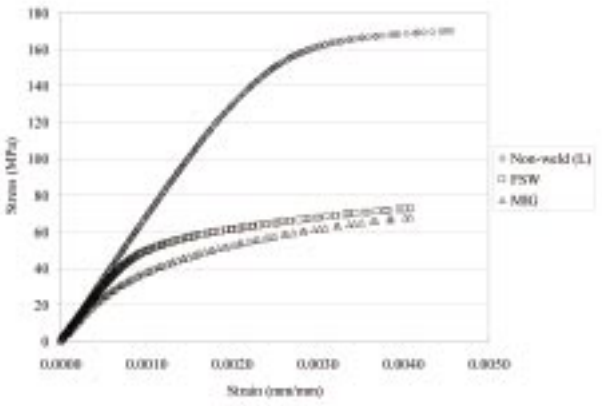

Fig. 4. Representative stress-strain curves for each weld condition and baseline material

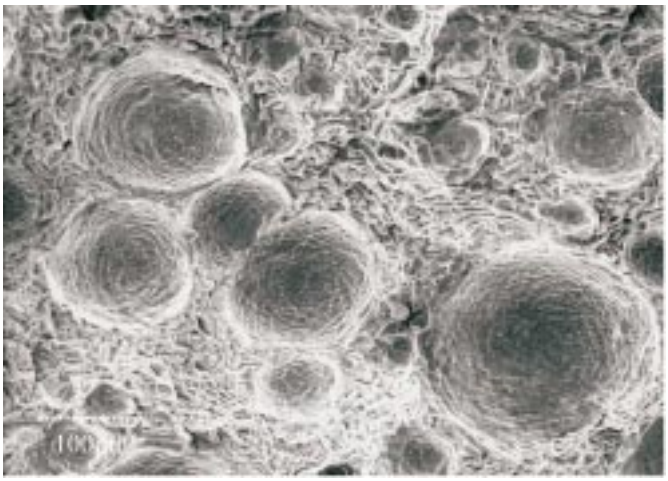

Fig. 5. SEM micrograph of representative MIG weld fracture surface showing voids

It is of particular interest to note that all FSW tensile specimens failed on the retreating side of the weld, approximately 10 mm from the center. This occurred despite the fact that tensile loading on the retreating side was in the L-direction, the strongest orientation, and on the advancing side, loading was in the LT-direction, the weaker orientation. Other research studies on aluminum alloys 6063-T5 and 7075-T651 observed a similar phenomenon [15, 16]; however, the welds in those investigations were traditional butt welds, and tensile loading was in the LT-direction on both the retreating and advancing sides. The MIG welded tensile specimens did not demonstrate such as systematic failure mode, with fractures seen on both sides of the weld. Electron microscopy of the FSW specimens, therefore, examines the fracture behavior of the retreating side. Figure 6a is an SEM micrograph of a representative FSW fracture surface. When compared to the MIG weld micrograph, a higher weld quality is immediately noted. No voids are present on the fracture surface other than the dimples caused by microvoid coalescence, a characteristic of ductile rupture. Clearly, this fracture surface indicates a greater degree of ductility and is consistent with the enhanced mechanical properties achieved through FSW than by MIG welding. The nucleation source for the microvoids, however, is unclear. Very few secondary phase particles are evident on the FSW fracture surface through SEM, though some iron, silicon containing particles (Fe_xSiAl_y) are seen in the dimples as shown in Figure 6b (approximate particle diameter is 5 μm). The dimples, therefore, may nucleate around the large particles present in the 6101 alloy.

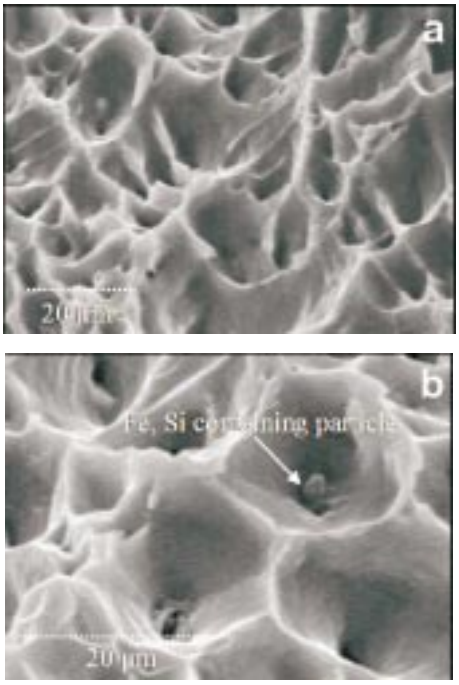

Fig. 6. a) SEM micrograph of representative FSW weld fracture surface showing ductile rupture and b) Higher magnification of same area highlighting iron, silicon containing particle in dimple

Optical micrographs of the FSW nugget show a coherent microstructure composed of small grains free of the defects commonly seen in fusion welding. The FSW microstructure, therefore, is consistent with the greater mechanical properties determined for the FSW speci-

mens when compared to the MIG welded specimens. A micrograph of a representative FSW nugget is shown in Figure 7 with the retreating and advancing sides indicated. The complex flow pattern of the FSW process is clearly evident and highlighted by the banded microstructure dominating the weld nugget. The spacing of the bands is directly related to the advance of the tool per revolution [17]. The higher magnification image of the nugget shown in Figure 8 reveals that the grain size is approximately equivalent in both the "light" and "dark" bands and varies between 10 μm and 20 μm and was smaller than in base material by an order of magnitude. The contrast between the two bands results from an uneven distribution of secondary phase particles. The dark band contains numerous, coarsened particles along the grain boundaries and in the grain, while the light band has relatively few particles. This microstructural characteristic is discussed in greater detail in the proceeding section.

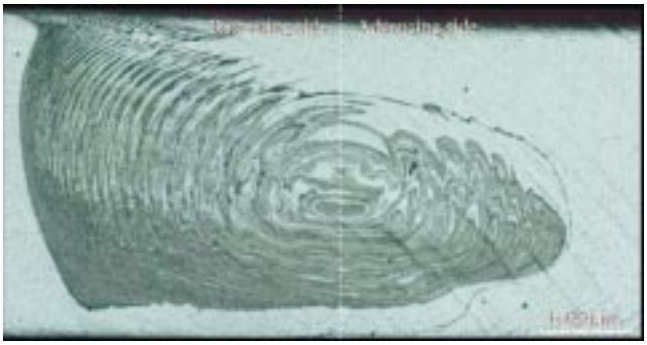

Fig. 7. Optical micrograph of representative FSW nugget showing the typical banded structure

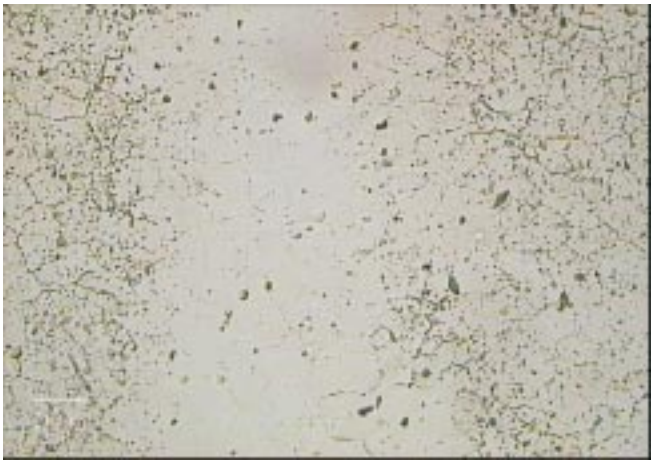

Fig. 8. Optical micrograph of banded structure revealing uneven particle distribution between bands, but equivalency in grain size

4. Discussion

When comparing MIG welding and FSW of aluminum 6101-T6 extrusions, friction stir welding produces a higher quality weld with superior mechanical properties. The FSW tensile specimens exhibit greater ductility than the MIG welded specimens and show the elastic-plastic stress-strain behavior common to aluminum alloys. FSW, itself, is a much less invasive process than conventional fusion welding so these observations are not surprising. During MIG welding the workpieces undergo melting and re-solidification, whereas FSW simply capitalizes on plastic flow in the extrusions to form the weld. Failure of all FSW tensile specimens on the retreating side despite loading on that side occurring in L-direction suggests that mechanical performance is independent of initial extrusion and grain elongation. The action of the FSW tooling consistently establishes conditions on the retreating side that lead to preferential failure.

Residual stress also contributes to the preferential failure on the retreating side. Several investigations of other aluminum alloys have shown that residual stress following FSW is consistently higher on the retreating side of the weld than on the advancing side [18–20]. If a residual stress is present, then the magnitude of the shear stress on the planes 45° to the tensile axis is increased, and the applied load required for tensile failure is reduced. During tensile testing, therefore, failure conditions are first realized on the retreating side of the weld where the residual stress is greater. The exact mechanisms leading to a greater residual stress state on the retreating side are not fully understood, but a qualitative understanding comes from examining the tool rotation and the weld direction. On the advancing side of the weld, the tool rotation is coincident with the tool advance, primarily deforming material along the weld direction. On the retreating side of the weld, however, the tool rotation opposes the tool advance and primarily shears the material surrounding the rotating tool and results in a greater degree of residual stress.

Within the FSW nugget, a periodic particle density produced the observed banded structure, the "dark" bands reflecting a high particle density and the "light" bands reflecting a low one. The grains, themselves, show little deformation or elongation in the flow direction, suggesting that recrystallization has occurred. Interestingly, the grain size in both bands was equivalent, approximately 10 μm to 20 μm. This observation differs from other studies of aluminum alloys under similar welding conditions [15, 16]. In these investigations, the authors concluded that fine, equiaxed recrystallized grains comprised the dark bands, and coarse recrystallized grains comprised the lighter bands. Both of the studies examined aluminum alloys other than 6101-T6 and utilized a different weld geometry. Sutton et al. [17], however, noted the periodic particle density in their work on aluminum alloy 2024-T351 rolled sheet, concluding

that the dark bands were rich in Cu, Fe, Mg, and Mn particles and that the light bands were poor in these phases [21]. The exact reason for the uneven particle distribution is unknown at the stage. The particle distribution may arise from a segregation created by the flow patterns of the FSW process. Perhaps the bands represent a non-uniform temperature profile across the nugget, the light bands reflecting a higher temperature and supersaturation, and the dark bands reflecting a lower temperature and particle coarsening.

5. Conclusions

1. Friction stir welding produces a higher quality weld than MIG welding with superior mechanical properties. While the fracture surfaces of the MIG welds exposed numerous voids, the FSW fracture surfaces showed no welding defects and displayed the characteristics typical of ductile rupture.
2. All FSW tensile specimens failed on the retreating side of the weld demonstrating that mechanical performance is independent of the initial extrusion and grain elongation. The distribution of precipitates on the retreating side and the degree of residual stress are likely contributors to this failure behavior.
3. An uneven distribution of secondary phase particles creates the banded appearance of the FSW nugget. The "dark" bands reflect a high particle density, while the "light" bands reflect a low one. The grain size, however, in both bands is equivalent, between 10 μm to 20 μm and was smaller than in base material by an order of magnitude. Segregation created by the FSW flow patterns or a non-uniform temperature profile across the nugget may cause the observed particle distribution.

Acknowledgements

This research was financially supported by AGH University of Science and Technology, project no. 11.11.110.237.

REFERENCES

[1] W. M. Thomas, E. D. Nicholas, J. C. Needham, M. G. Murch, P. Templesmith, C. J. Dawes, G. B. Patent Application No. 9125978.8 (December 1991).
[2] C. Dawes, W. Thomas, TWI Bulletin 6, 124, November/December 1995.
[3] R. Braun, L. Lityńska-Dobrzyńska, Materials Science Forum **396-402**, 1531 (2002).
[4] L. Lityńska, R. Braun, G. Staniek, C. Dalle Donne, J. Dutkiewicz, Mat. Chem. Phys. **81**, 293 (2003).
[5] I. Shigematsu, K. Suzuki, T. Imai, Y.-J. Kwon, N. Saito, J. Mat. Sci. **40**, 2971 (2005).
[6] M. Dumont, A. Steuwer, A. Deschamps, M. Peel, P. J. Withers, Acta Met. **54**, 4793 (2006).
[7] R. S. Mishra, Z. Y. Ma, Mat. Sci. Eng. **R 50**, 1 (2005).
[8] M. A. Sutton, B. Yang, A. P. Reynolds, J. Yan, Mat. Sci. Eng. **A 364**, 66 (2004).
[9] B. J. Dracup, W. J. Arbegast, in: Proceedings of the 1999 SAE Aerospace Automated Fastening Conference & Exposition, Memphis, TN, October 5–7, 1999.
[10] A. von Strombeck, J. F. dos Santos, F. Torster, P. Laureano, M. Kocak, in: Proceedings of the First International Symposium on Friction Stir Welding, Thousand Oaks, CA, USA, June 14–16, 1999.
[11] ASTM B 317: Standard Specification for Aluminum-Alloy Extruded Bar, Rod, Tube, Pipe, and Structure Profiles for Electrical Purposes (Bus Conductor).
[12] W. M. Thomas, E. D. Nicholas, S. D. Smith, S. K. Das, J. G. Kaufman, T. J. Lienert (Eds.), Aluminum 2001 – Proceedings of the TMS 2001 Aluminum Automotive and Joining Sessions, TMS, 213, 2001.
[13] W. M. Thomas, K. I. Johnson, C. S. Wiesner, Adv. Eng. Mater. **5**, 485 (2003).
[14] ASTM E 8: Standard Test Methods for Tension Testing of Metallic Materials.
[15] M. W. Mahoney, C. G. Rhodes, J. G. Flintoff, R. A. Spurling, W. H. Bingel, Metall. Mater. Trans. **A 29**, 1955 (1998).
[16] Y. S. Sato, S. H. C. Park, H. Kokawa, Metall. Mater. Trans. **A 32**, 3023 (2001).
[17] M. A. Sutton, B. Yang, A. P. Reynolds, J. Yan, Mat. Sci. Eng. **A 364**, 55 (2004).
[18] M. James, M. Mahoney, Proceedings of the First International Symposium on Friction Stir Welding, Thousand Oaks, CA, USA, June 14–16, 1999.
[19] C. D. Donne, E. Lima, J. Wegener, A. Pyzalla, T. Buslaps, in: Proceedings of the Third International Symposium on Friction Stir Welding, Kobe, Japan, September 27–28, 2001.
[20] M. Peel, A. Steuwer, M. Preuss, P. J. Withers, Acta Mater. **51**, 4791 (2003).
[21] M. A. Sutton, B. Yang, A.P. Reynolds, R. Taylor, Mat. Sci. Eng. **A 323**, 160 (2002).

Received: 20 September 2006.